

Investigation of mechanosynthesized Fe<sub>50</sub>Ni<sub>40</sub>Al<sub>10</sub> powdersF. Hade<sup>a,\*</sup>, A. Otmani<sup>a</sup>, A. Djekoun<sup>b</sup>, J.M. Grenèche<sup>c</sup><sup>a</sup> Laboratoire de Recherche sur la Physico-Chimie des Surfaces et Interfaces, LRPCSI, Université 20 Août 1955, BP 26, Route d'El-Hadaiek, Skikda 21000, Algeria<sup>b</sup> Laboratoire de Magnétisme et Spectroscopie des Solides, LM2S, Université Badji Mokhtar, BP 12, Annaba 23000, Algeria<sup>c</sup> LUNAM, Université du Maine, Institut des Molécules et Matériaux du Mans, UMR CNRS 6283, 72085 Le Mans, France

## ARTICLE INFO

## Article history:

Received 18 September 2012

Received in revised form

22 April 2013

Available online 15 May 2013

## Keywords:

Nanostructure

Mechanical alloying

Powder diffraction

Mössbauer spectroscopy

## ABSTRACT

The synthesis of Fe<sub>50</sub>Ni<sub>40</sub>Al<sub>10</sub> powder mixture has been performed in a high-energy planetary ball mill. The phase transformations and structural changes occurring during mechanical alloying were investigated by X-ray diffraction (XRD) and Mössbauer spectroscopy. XRD analysis and Rietveld method revealed the formation of a single nanocrystalline fcc  $\gamma$ -Ni(Fe,Al) solid solution with a lattice parameter close to  $a_{\gamma\text{-Ni(Fe,Al)}} = 0.3612$  nm, after 4 h of milling. The final powder is characterized by an average crystallite size of 14 nm accompanied by the introduction of a lattice strain of order of 1.37%. These values are markedly higher than those reported for mechanically alloyed Fe<sub>50</sub>Ni<sub>50</sub> powders. It was found that the formation of the bcc phase, which coexisted with the fcc structure in the Fe–Ni phase diagram, was inhibited. However, mechanical alloying process gives rise to the Ni<sub>3</sub>Al intermetallic phase, at the early stages of milling. Mössbauer spectroscopy showed that all powders exhibited a ferromagnetic behavior and no paramagnetic phase was detected. The addition of low aluminium content caused more broadening of hyperfine field distributions and lower magnetic field due to the diffusion of Al atoms into  $\gamma$ -FeNi lattice.

© 2013 Elsevier B.V. All rights reserved.

## 1. Introduction

In the recent years, Iron–Nickel alloys have generated a lot of interest in both fundamental and applied science. They belong to the soft-magnetic materials and are widely used in the industrial applications. Fe–Ni materials are easily magnetized till saturation by weak fields; they exhibit narrow hysteresis loops, low coercive fields, small magnetic losses and good anticorrosion properties. Besides that, they show anomalies of some physical properties which take place when the iron concentration changes around the Invar region (Fe<sub>65</sub>Ni<sub>35</sub>). Due to these reasons, intensive researches were carried on the reaction process of Fe–Ni binary system; evaporation [1,2], chemical methods [3,4] electrodeposition [5,6] and mechanical alloying route [7–15]. The latter was applied to a broad range of Ni concentrations [9,16–18], milling conditions [18–20] and martensitic transformation [21,22]. It has been reported that the addition of alloying element to Fe–Ni alloys could potentially influence their physical properties in a significant manner [23–25]. Consequently, MA of Fe–Ni based alloys has been the subject of a considerable number of studies; Fe–Ni–Mg [26–28], Fe–Ni–Cu [29,30], Fe–Ni–Co–Zr–B [31,32], Fe–Ni–Cu–Co [33,34]. However, few published works concerning MA process of ternary Fe–Al–Ni powders have been conducted [35–37].

The present work is dedicated to the study of the structural and hyperfine interactions of mechanically alloyed Fe<sub>50</sub>Ni<sub>40</sub>Al<sub>10</sub> powders

by means of combined X-ray diffraction and Mössbauer spectroscopy techniques. We would like to emphasize that an attempt is done in order to delineate the influence of low aluminium content when it is added to mechanically alloyed Fe<sub>50</sub>Ni<sub>50</sub> powders. A comparative investigation of structural and microstructural properties of mechanosynthesized Fe<sub>50</sub>Ni<sub>40</sub>Al<sub>10</sub> powders with those of published MA Fe<sub>50</sub>Ni<sub>50</sub> was carried out.

## 2. Experimental procedure

## 2.1. Processing

Elemental Fe, Ni and Al powders with purity of 99.99% were weighed and mixed to obtain the desired composition of Fe<sub>50</sub>Ni<sub>40</sub>Al<sub>10</sub>. The milling was carried out using a planetary high-energy ball mill (Fritsch Pulverisette 7). The powders were introduced into cylindrical steel vials with four steel balls ( $\Phi$ , 10 mm; mass, 7 g). The vials were filled with high purity argon gas to avoid atmospheric contamination. The ball-to-powder weight ratio was 14:1. The powders were milled for several periods  $\leq 12$  h. To avoid excessive heating during milling, each 15 min of milling was followed by a stay during 15 min.

## 2.2. Characterization

The phases formed and their associated structural and microstructural properties were investigated by X-ray diffraction (XRD)

\* Corresponding author. Tel./fax: +213 38 75 29 11.  
E-mail address: [hade77@yahoo.fr](mailto:hade77@yahoo.fr) (F. Hade).

and Mössbauer spectroscopy. XRD measurements were conducted using a Siemens D501 diffractometer with Cu  $K_{\alpha 1}$  radiation, in the  $2\theta$  range from  $35^\circ$  to  $90^\circ$  by step of  $0.02^\circ$ . The obtained patterns were fitted using the Maud program based on the Rietveld method [38], which has proved to be an extremely powerful tool for the characterization of fine-grained samples [37,39].

In order to give more accurate description of the hyperfine properties, the powders were investigated by  $^{57}\text{Fe}$  Mössbauer spectrometry (MS). The MS measurements were performed at 300 K in transmission geometry, using a constant acceleration signal spectrometer with a  $^{57}\text{Co}$  source diffused into rhodium matrix. Mössbauer spectra were fitted using the Mosfit computer program [40], a least-square iteration program. It was found that the best numerical fittings were achieved when hyperfine field distributions,  $P(B_{\text{hf}})$ , were used. The isomer shift values are quoted relative to that of  $\alpha\text{-Fe}$  at 300 K.

### 3. Results and discussion

#### 3.1. XRD analysis

##### 3.1.1. Phase constitution of as-milled powders

Fig. 1(a) shows the evolution of the diffraction patterns of MA  $\text{Fe}_{50}\text{Ni}_{40}\text{Al}_{10}$  powders as a function of milling time.

The XRD pattern of the sample milled for 0.25 h reveals the presence of the starting elements with a reduced intensity of Al peaks, probably due to its small percentage and low atomic number in comparison with those of Fe and Ni [41,42]. About 0.25 h later, only the diffraction Bragg peaks of Fe and Ni are present. After 1 h of milling, besides the increase in the line broadening which is due to both the reduction in crystallite size and increase in microstrains, new peaks occur on the left side of fcc XRD lines, which are characteristic of the  $\text{Ni}_3\text{Al}$  intermetallic phase.

$\text{Ni}_3\text{Al}$  crystallizes in an ordered fcc ( $L1_2$ ) superstructure (AuCu<sub>3</sub> type), its space group is  $Pm\bar{3}m$  [43]. It has been shown that  $\text{Ni}_3\text{Al}$  is ordered to very near its melting point [44]. It exists over a wide range of Al concentration (24–27 at%). The unit cell of  $\text{Ni}_3\text{Al}$  can be visualized as an ordered cubic structure with the Al atoms

occupying corners of the cube and the Ni atoms located at the cube faces in the lattice. Synthesis of  $\text{Ni}_3\text{Al}$  intermetallic phase by MA has been previously reported [45–51]. Enayati et al. [45] have shown that MA of Ni and Al powders first resulted in a Ni(Al) solid solution which transformed to the disordered  $\text{Ni}_3\text{Al}$  intermetallic compound with nanocrystalline structure on further milling. Lu et al. [51] have pointed out that the formation of  $\text{Ni}_3\text{Al}$  using MA was through a diffusion process in which atomic movements constitute diffusion by vacancy mechanism.

Since there is no interdiffusion between Fe and Ni, in the early stages of milling, we can assume that Al will first react with Ni leading to the formation of  $\text{Ni}_3\text{Al}$ . The enthalpy of formation of this phase is approximately  $-35$  kJ/mol [52], we strongly deduce that the energy released by the planetary mill was sufficient to induce the formation of  $\text{Ni}_3\text{Al}$ . On the other hand, during MA process, several factors like temperature of powders, density of defects such as dislocations and vacancies, reduced crystalline size [53–54] can effectively affect the diffusion process. Synthesis of intermetallic phases was previously reported in the works of Hadeef et al. [37,55] during the milling process of ternary  $\text{Fe}_{50}\text{Al}_{40}\text{Ni}_{10}$  powders. After 4 h of milling, Fe peaks disappear without displacement, indicating the formation of a fcc  $\gamma\text{-Ni(Fe,Al)}$  solid solution and at the same time the most intense peak is shifted to lower angles side (Fig. 1(b)). Further milling does not give rise to a significant change in the XRD pattern.

In the case of ball milled  $\text{Fe}_{50}\text{Ni}_{50}$  powders, the authors reported the formation of a fcc  $\gamma\text{-FeNi}$  phase called taenite which coexisted with a bcc structure (kamacite), in the Fe–Ni phase diagram [9–11,13,56]. In this study, the formation of both bcc and fcc phases is not observed, but only the fcc one is obtained. Djekoun et al. [13] have mentioned the formation of a fcc phase in the early stages of milling while the bcc structure was obtained after 48 h. Similar results have been found by Khurt et al. [56]. Whereas Guittoum et al. [14] have mentioned that only the fcc phase was synthesized. Many works have reported that the concentration ranges of the bcc and fcc single-phase solid solutions depend on the milling intensity and shift to low nickel concentration at an increase in the milling intensity [8,10,18,56].

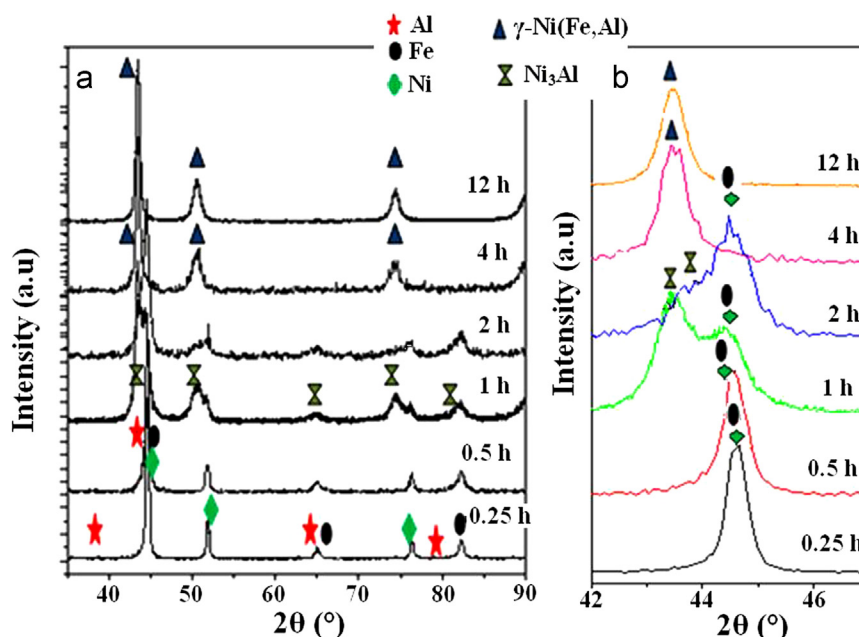


Fig. 1. (a) XRD patterns of mechanically alloyed  $\text{Fe}_{50}\text{Ni}_{40}\text{Al}_{10}$  powder and (b) evolution of the most intense peak, as a function of milling time.

3.1.2. Structural and microstructural properties

As mentioned above, the diffraction patterns were fitted using the Maud program [57], which is based on the Rietveld method [38] combined with a Fourier analysis. This procedure is well adapted for diffraction patterns which exhibit broadened diffraction peaks. Indeed, this method allows the refinement of the structural and microstructural parameters; the lattice parameters, the size and the microstrains of crystalline domains. In this section, the obtained results are discussed and compared with published structural and microstructural characteristics of MA Fe<sub>50</sub>Ni<sub>50</sub> alloy. Table 1 summarizes published data on this material.

Fig. 2 shows the variation of the lattice parameters as a function of milling time.

The lattice parameter of iron varies slightly between 0 and 2 h of milling from its initial value ( $a=0.2866$  nm) to  $a_{2h}=(0.2871 \pm 0.0001)$  nm (Fig. 2(a)), in good agreement with the result reported by Mhadhbi et al. [59], in the case of ball milled pure iron. The increase in lattice parameter is probably caused by the grain expansion due to the increase in the density of dislocations with their characteristic strain fields [59,60] as well as the high concentration of point defects induced by milling process [61].

A linear increase of lattice parameter is observed for Ni. It strongly increases during the first 4 h of milling to  $a_{4h}=(0.3621 \pm 0.0002)$  nm. It is worth noticing that this elevated value is obtained when the fcc  $\gamma$ -Ni(Fe,Al) solid solution is completely formed. After 12 h, the lattice parameter shows a slight reduction thereafter it reaches a value close to  $a=(0.3612 \pm 0.0002)$  nm. This value is higher than those reported for MA FeNi, as seen in Table 1. It is important to emphasize that the obtained value is also greater than those corresponding to Fe<sub>50</sub>Ni<sub>50</sub> alloys prepared by other manufacturing processes; Liu et al. [62] reported a value close to  $a=0.359$  nm, for samples prepared by evaporation in nitrogen atmosphere. A nearly value of  $a=0.3578$  nm was mentioned by Kadziolka-Gawel et al. [63], for polycrystalline Fe<sub>50</sub>Ni<sub>50</sub> alloys. In the previous studies, the formation of Fe<sub>50</sub>Ni<sub>50</sub> alloy takes place when Fe atoms diffused into Ni lattice. The abrupt increase in the lattice parameter of our samples can be reasonably

explained as a result of replacement by aluminium atoms which have a larger atomic radius ( $R_{Al}=0.142$  nm) than Fe and Ni of some sites of Fe atoms ( $R_{Fe}=0.127$  nm) in the fcc NiFe crystal lattice (Ni and Fe atoms have nearly identical atomic radii in the solid state).

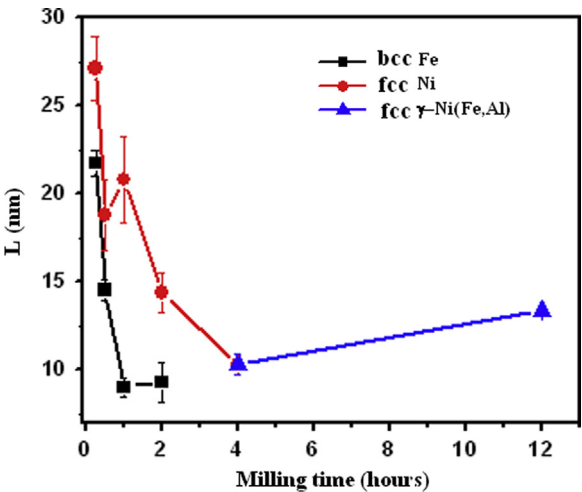
**Ni<sub>3</sub>Al phase:** Ni<sub>3</sub>Al and Ni have the same crystal structure and the lattice parameter of Ni<sub>3</sub>Al differs only by 1% of that of Ni. In this study, the value of lattice parameter of Ni<sub>3</sub>Al increases from  $a_{Ni3Al}=(0.355 \pm 0.0001)$  nm, for 1 h to  $a_{Ni3Al}=(0.3610 \pm 0.0001)$  nm, for 2 h of milling, mainly caused by the presence of point defects. It has been found that the formation energy of vacancies or interstitials is about two times higher than that of the antisite defects in Ni<sub>3</sub>Al [64]. It is reasonably supposed that the most point defects take form of antisite defects.

Fig. 3 presents the evolution of the crystallite sizes of milled Fe<sub>50</sub>Ni<sub>40</sub>Al<sub>10</sub> powders.

The crystallite sizes decrease after 0.25 h of milling to 22 and 27 nm for Fe and Ni, respectively. As evident from the figure, the corresponding decrease of iron crystallites is extremely high and reaches a value of about 9 nm, after 2 h of milling. It is important to note that the average crystallite size of Fe is always less than that of Ni, at different stages of milling. Valderruten et al. [11] have shown in milled FeNi powders, where the fcc and bcc phases coexisted, that the crystallite size of the fcc phase was always greater than that of the bcc one. This difference is attributed to the fragile and ductile character of bcc and fcc phases, respectively. At the end of milling, the crystallite size of  $\gamma$ -Ni(Fe,Al) solid solution is close to 14 nm. This value is higher than those reported by some

**Table 1**  
Summary of structural and microstructural properties of MA Fe<sub>50</sub>Ni<sub>50</sub>; lattice parameter:  $a$ , average crystallite size;  $\langle L \rangle$ , lattice strains;  $\langle \sigma^2 \rangle^{1/2}$ .

Research groups	Structural and microstructural properties		
	$a$ (nm)	$\langle L \rangle$ (nm)	$\langle \sigma^2 \rangle^{1/2}$ (%)
Djekoun et al. [13]	0.3601	5	0.5
Guittoum et al. [14]	0.3597	12.9	0.41
Jartych et al. [15]	0.3594	10	0.5
Pekala et al. [58]	0.3591	14	0.5



**Fig. 3.** Evolutions of the average crystallite size of Fe<sub>50</sub>Ni<sub>40</sub>Al<sub>10</sub> powder as a function of milling time.

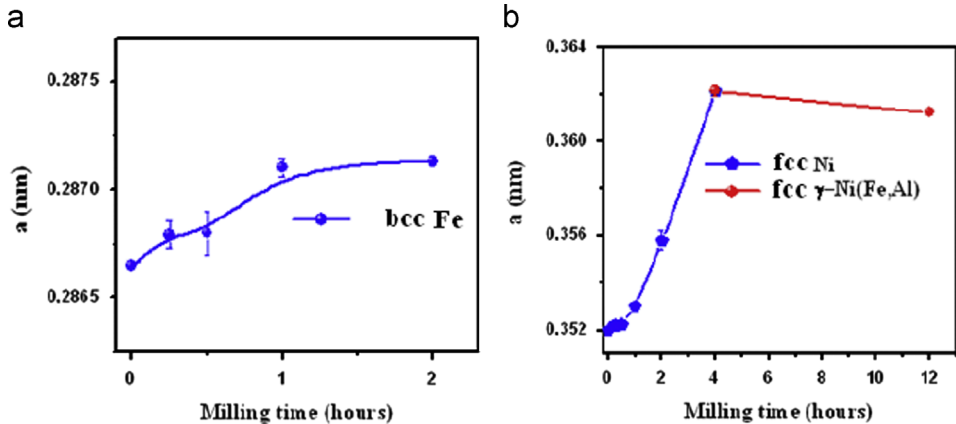


**Fig. 2.** Evolutions of the lattice parameter Fe<sub>50</sub>Ni<sub>40</sub>Al<sub>10</sub> powder as a function of milling time.

researchers (see Table 1). It may also be noted that the crystallite size currently obtained is even elevated as compared with mechanically alloyed Fe–Ni based alloys:  $\text{Fe}_{50}\text{Ni}_{38}\text{B}_{18}\text{Mo}_4$  (6 nm) and  $\text{Fe}_{42}\text{Ni}_{40}\text{B}_{18}$  (7.4 nm) [65]. This suggests that the crystallite size is strongly influenced by the presence of aluminium content.

In Fig. 4, the evolutions of the lattice strain as a function of milling time are illustrated. One can see that the lattice strains become gradually higher with increasing milling time, for both Fe and Ni. For iron,  $\langle\sigma^2\rangle^{1/2}$  changes from the initial value of  $(0.314 \pm 0.012)\%$  to a value close to  $(1.086 \pm 0.021)\%$  after 2 h of milling. A similar behavior, increased lattice strain with increasing lattice parameter, is observed, for Ni. It increases rapidly to  $(1.819 \pm 0.232)\%$  then it decreases slowly when the  $\gamma\text{-Ni(Fe,Al)}$  solid solution is formed, reaching a value of  $(1.371 \pm 0.232)\%$ , at the end of MA process.

One can see that the lattice strain value obtained in the present investigation is much higher than those reported by other investigators (see Table 1). It is widely accepted [66] that lattice strain may arise from mechanical deformation induced by repeated ball-to-powder collisions upon milling, from an increasing grain boundary fraction. It is well established that the smaller the grain size, the higher the grain boundary contribution is; however, the crystallite size obtained by us is higher than others previously reported. Consequently the size effect cannot be invoked to explain the observed enhancement of lattice strain as compared with experimental published data. The last contribution is due to the difference in atomic sizes of the elemental powders. Indeed, Ni and Fe are closely situated in the Mendeleev periodic table of elements and have identical atomic radii ( $R_{\text{Fe}}=0.127$  nm,  $R_{\text{Ni}}=0.125$  nm) however aluminium ( $R_{\text{Al}}=0.142$  nm) has a relatively large atomic radius as compared to Fe and Ni. We can conclude that the introduction of Al into  $\gamma\text{-FeNi}$  induced stronger distortion of the crystal lattice. It seems that the last contribution is the main cause of the enhanced lattice strain obtained in the present investigation.

### 3.2. $^{57}\text{Fe}$ Mössbauer spectroscopy

#### 3.2.1. Mössbauer spectra characteristics

Due to the sensitivity of Mössbauer spectroscopy to local order on an atomic scale, this technique has been an important tool in investigating Fe–Ni phases in prepared samples [3,8–15].

The Mössbauer spectra of mechanically alloyed  $\text{Fe}_{50}\text{Ni}_{40}\text{Al}_{10}$  powders are displayed in Fig. 5. They illustrate perfectly the ferromagnetic character of the powders, without presence of any paramagnetic phase. As one can see, the spectra reveal gradual

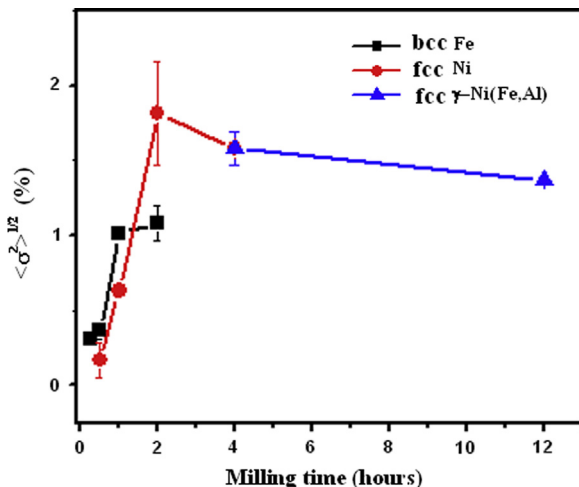


Fig. 4. Evolutions of lattice strain of  $\text{Fe}_{50}\text{Ni}_{40}\text{Al}_{10}$  powder as a function of milling time.

mixing of the elemental powders when increasing milling time. It should be noted that the magnetic sextets of the investigated samples are asymmetric, for milling times longer than 2 h, which is associated to the existence of a correlation between the isomer shift and the hyperfine field, for each Fe site.

The Mössbauer spectra of the powders milled for 0.5 and 1 h are almost identical and are fitted with three discrete sextets: a sextet with narrow lines, with an hyperfine field  $B_{\text{hf}}=33$  T and isomer shift (IS)=0.00 mm/s, originating from the  $\alpha\text{-Fe}$ , and two minor sextets with hyperfine fields smaller than 33 T. Increasing milling time to 2 h, the spectrum is fitted with three discrete sextets and an hyperfine field distribution,  $P(B_{\text{hf}})$ . For times  $\geq 4$  h, the spectra consist of a broad magnetic sextet where the magnetic hyperfine field is distributed due to the multiplicity of local environments in which iron atoms are widely and randomly substituted by those of Al and/or Ni ones. It has been reported that the lines observed for iron–nickel alloys were not much broader than those of pure iron. The relative small broadening found in FeNi alloys is qualitatively understandable since they dissolve with large magnetic moments of their own, so that the replacement of an iron atom does not produce a large local disturbance [67]. Based on the physics of MA process, the

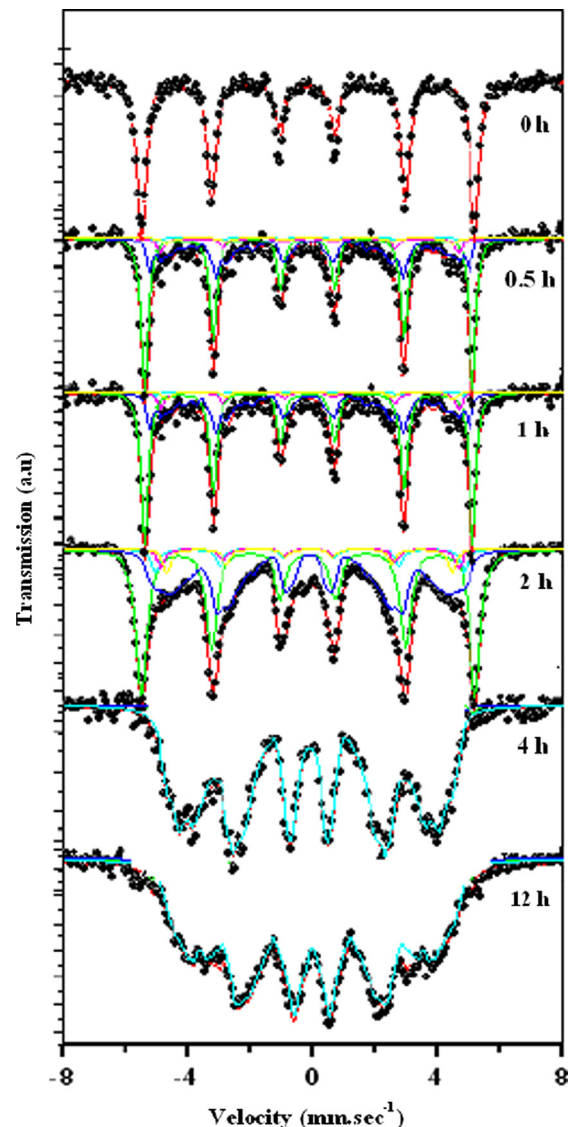


Fig. 5. Room temperature  $^{57}\text{Fe}$  Mössbauer effect spectra of mechanically alloyed  $\text{Fe}_{50}\text{Ni}_{40}\text{Al}_{10}$  powder as a function of milling time.



broadening of the spectral lines as compared to those of  $\alpha$ -Fe, resulted from the alloying process and also from the reduction of the grain sizes accompanied by high lattice strain [68], in good agreement with the XRD results. The formation of a paramagnetic phase in mechanically alloyed  $\text{Fe}_{50}\text{Ni}_{50}$  was previously mentioned; Djekoun et al. [13] reported the emergence a paramagnetic  $\gamma$  (fcc) FeNi phase with a concentration of about  $\approx 30$  at% Ni. Guittoum et al. [14] also reported the appearance of a paramagnetic component which was attributed to a fcc iron rich paramagnetic phase that usually coexisted with the ferromagnetic fcc around 50% Fe.

The evolution of the hyperfine field distributions  $P(B_{\text{hf}})$  as a function of milling time is shown in Fig. 6. The hyperfine field distributions  $P(B_{\text{hf}})$  of the powders milled for 0.5 and 1 h are identical and have the shape of a simple Gaussian function centered on  $\sim 33$  T, which corresponds to  $\alpha$ -Fe. A weaker contribution at low fields is reported, when increasing milling time to 2 h. For milling times  $\geq 4$  h,  $P(B_{\text{hf}})$  are mostly similar; both peak broadening and shift towards low fields are observed. One can see that they can be considered to be the envelope of a number of overlapping subspectra, in which the most probable hyperfine magnetic fields for both 4 and 12 h of milling, are 24 T originating from the fcc  $\gamma$ -Ni(Fe,Al) solid solution. Besides, it is important to note that the  $P(B_{\text{hf}})$  corresponding to the sample milled for 12 h, includes a significant contribution in the low fields. This latter is probably due to Fe atoms situated in the grain boundaries. Hadeef et al. [69] have reported in mechanically milled  $\text{Fe}_{50}\text{Al}_{40}\text{Ni}_{10}$  that the low hyperfine field values ( $< 15$  T) resulted from Fe atoms located in the disordered grain boundaries. The thickness of grain

boundaries was estimated at about 0.5 nm (two atomic layers) in fcc Fe–Ni alloys [70,71].

By comparing the obtained hyperfine field distributions with those published for MA  $\text{Fe}_{50}\text{Ni}_{50}$ , a noticeable broadening is observed. The broadening of  $P(B_{\text{hf}})$  is generally interpreted in terms of disordered systems and presence of defects in milled alloys [13,15]. But these reasons are not enough to explain the increased broadening, since all samples were prepared by the same process. It has been reported that the broadening of Mössbauer spectra of Fe–Al represents the spread in the values of the hyperfine field due to the local fluctuations of composition throughout the alloy [67], whereas the presence of Ni does not cause such changes as described above. This can be translated in  $P(B_{\text{hf}})$  as follows; the presence of numerous types of Fe–Al configurations distributed the intensities around each position of the hyperfine magnetic field and thus collapse to a broad line.

### 3.2.2. Hyperfine parameters

Fig. 7 shows the evolution of the hyperfine interactions parameters obtained from the fitting of the experimental spectra of MA  $\text{Fe}_{50}\text{Ni}_{40}\text{Al}_{10}$  powders.

One can see the decrease of the average hyperfine field when milling time increases; this can be attributed to the substitution of Fe atoms by Al and/or Ni ones. At the end of milling, the hyperfine field is close to 20 T. We should point out that  $\langle B_{\text{hf}} \rangle \neq B_{\text{hf}}$ , where  $B_{\text{hf}}$  is the value of the most probable field. This result confirms our earlier suggestion concerning the asymmetric shape of Mössbauer spectra recorded for prolonged milling times. It is important to note that this value is much lower than those reported in literature for MA  $\text{Fe}_{50}\text{Ni}_{50}$ ; 30.5 T [58], 30.8 T [9,14,72,73], 31 T [74], 31.5 T [15], 31.2 T [13]. The observed differences can be qualitatively explained by the local environment model [75], in which the magnetic moment of an element depends on the number of nearest neighbors (NN). For fcc Fe–Ni alloys, it is assumed that one Ni atom increases the hyperfine field at  $^{57}\text{Fe}$  site by  $\Delta B_1 = 1.08$  T when it substitutes iron atom in the first coordination sphere and decreases it by  $\Delta B_2 = -0.34$  T, in the second sphere [76]. For Fe–Al alloys, Stearns [77] has proposed that the hyperfine field at the Fe site decreases linearly with the number of Al atoms in the first and second neighboring spheres. For each Fe atom in the first shell substituted by Al, there is a reduction of  $\Delta B_1 = 2.4$  T in the hyperfine field of pure Fe; similarly for each one of the second sphere results in a decrease of  $\Delta B_2 = 1.1$  T. Using this simple model, with a simplifying assumption that only the nearest neighbors were taken into account because merely replacement of Fe atom in nearest neighborhood (NN) has strong influence and may be registered with high reliability. We strongly deduce that the reduced value of the hyperfine field is obtained only when there is diffusion of Al atoms into the first coordination sphere of Fe probe. This indicates that there is

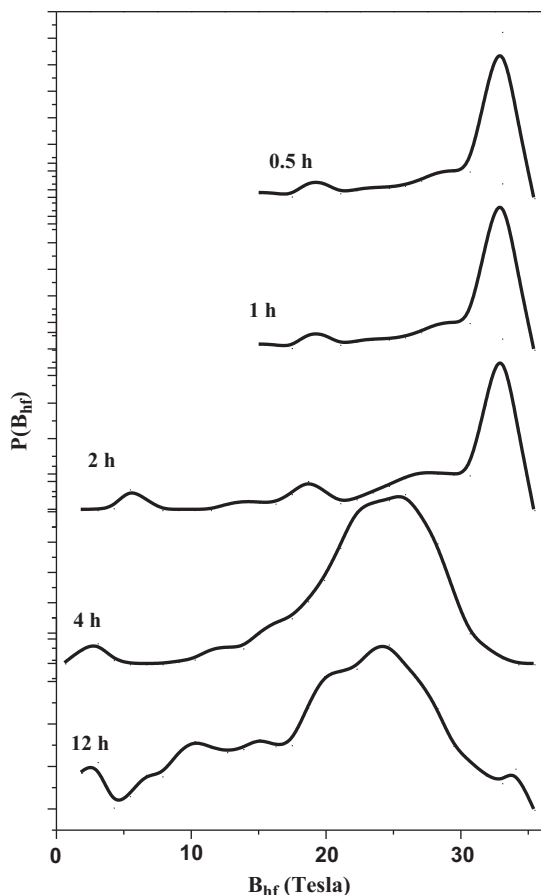


Fig. 6. Hyperfine field distributions,  $P(B_{\text{hf}})$ , of mechanically alloyed  $\text{Fe}_{50}\text{Ni}_{40}\text{Al}_{10}$  powder as a function of milling time.

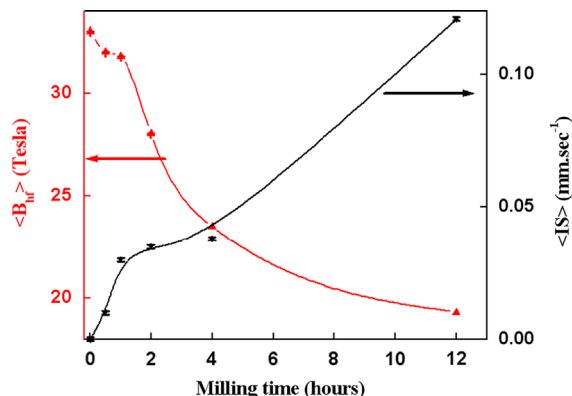


Fig. 7. Evolution of the hyperfine parameters  $\langle B_{\text{hf}} \rangle$  and  $\langle IS \rangle$ , as a function of milling time.

enrichment in Al rather than Ni, while the percentage of Ni is four times greater than Al. It has been reported that the diffusivity of the solute can be obtained from its melting point. The lower the melting point, the higher the diffusivity [52]. According to the thermodynamic data, Ni has a relatively high melting temperature (1455 °C) compared to that of Al (660 °C). It is known that melting temperature decreases with decreasing grain size. The latter effect is particularly significant for nanograins [78]. This result should certainly be considered to explain the observed features.

The average isomer shift is positive and increases with increasing milling time. This increase corresponds to a significant decrease in the  $s$  electron density at the  $^{57}\text{Fe}$  nucleus. After 12 h of milling, the isomer shift reached a value of  $\langle IS \rangle = 0.12$  mm/s. It is interesting to note that  $\langle IS \rangle$  increases while  $\langle B_{\text{hf}} \rangle$  decreases, when increasing the processing time. It has been reported that the electron charge density on the iron nucleus decreases upon alloying Ni into Fe as the average isomer shift increases with increasing Al and Ni [79]. In fact, there is no published result in literature regarding the isomer shift evolution, in the case of MA  $\text{Fe}_{50}\text{Ni}_{50}$ . However, a negative value close to  $\langle IS \rangle = -0.02$  mm/s was found by Lima et al. [80], for  $\text{Fe}_{50}\text{Ni}_{50}$  alloy synthesized by ultra rapid autocatalytic chemical reduction. Hadeef et al. [69] have mentioned a value of  $\langle IS \rangle = 0.112$  mm/s which provides a neighborhood between 4 and 4.5 aluminium atoms in mechanically alloyed  $\text{Fe}_{50}\text{Al}_{40}\text{Ni}_{10}$  powders, whereas five Ni atoms were located in the nearest neighborhood in mechanically milled Fe-50 at% Ni alloys, as proposed by Jartych et al. [15] and Pekala et al. [58].

#### 4. Conclusion

The mechanical alloying of Fe-40Ni-10Al powder mixtures has been attempted. At the early stage of MA, the energy released by the planetary mill is sufficient to induce the formation of  $\text{Ni}_3\text{Al}$  intermetallic phase. With increasing milling time to 4 h, a single nanostructured fcc  $\gamma\text{-Ni(Fe,Al)}$  solid solution was synthesized with a lattice parameter close to  $a_{\gamma\text{-Ni(Fe,Al)}} = 0.3612$  nm. The final powder is characterized by an average crystallite size of 14 nm accompanied by the introduction of a lattice strain of order of 1.37%. These values are markedly higher than those reported for published MA  $\text{Fe}_{50}\text{Ni}_{50}$ . In the present investigation, we have concluded that a small amount of added Al affects the structural and microstructural properties of the investigated samples mainly caused by the high atomic radii of Al atoms. In addition, our study clearly indicates that Al atoms should be the major origin of the lower hyperfine field and the increased isomer shift behaviors in the MA  $\text{Fe}_{50}\text{Ni}_{40}\text{Al}_{10}$  powders. The obtained value of 20 T indicates an enrichment in Al rather than Ni and provides an atomic environment where each Fe probe is surrounded by less than five Ni atoms in the nearest neighborhood.

#### Acknowledgments

This work was supported by the Ministère de l'Enseignement Supérieur et de la Recherche Scientifique, Algérie. The authors owe them deepest gratitude to A.M. Mercier, from the Laboratory of Fluorures, University of Maine, Le Mans (France), for performing X-ray diffraction measurements.

#### References

- [1] C. Duhamel, Y. Champion, M. Tencé, M. Walls, Synthesis of controlled-chemistry ultrafine  $\text{Fe}_x\text{Ni}_{1-x}$  ferromagnetic powders, *Journal of Alloys and Compounds* 393 (2005) 204–210.
- [2] Y.V. Baldokhin, P.Y. Kolotyrykin, Y.I. Petrov, E.A. Shafranovsky, On the exhibition of high and low spin states of the fcc phase in ultrafine Fe and Fe-Ni particles, *Physics Letters. A* 189 (1994) 137–139.
- [3] J.R. Enio Lima, D. Valderes, J.C. de Lima, P.F. Papaleo Fichtner, Nanocrystalline  $\text{Fe}_x\text{Ni}_{1-x}$  ( $x \leq 0.65$ ) alloys formed by chemical synthesis, *Journal of Alloys and Compounds* 396 (2005) 10–17.
- [4] Y.J. Suh, H.D. Jang, H. Chang, W.B. Kim, H.C. Kim, Size-controlled synthesis of Fe-Ni alloy nanoparticles by hydrogen reduction of metal chlorides, *Powder Technology* 161 (2006) 196–201.
- [5] S.H. Hsieh, J.J. Horng, Deposition of Fe-Ni nanoparticles on  $\text{Al}_2\text{O}_3$  for dechlorination of chloroform and trichloroethylene, *Applied Surface Science* 253 (2006) 1660–1665.
- [6] B. Schirmer, M. Wuttig, Antiferromagnetic coupling in fcc Fe overlayers on Ni/Cu(100), *Physical Review B* 60 (1999) 12945–12949.
- [7] P.J. Schilling, V. Palshin, R.C. Tittsworth, J.H. He, E. Ma, Overlapping solubility in mechanical alloyed Fe-Ni and Fe-Cu, *Physical Review B* 68 (2003) 224204–224209.
- [8] S.D. Kaloshkin, V.V. Tcherdyntsev, A. Tamin, Y.V. Baldokhin, E.V. Shelekhov, Phase transformations in Fe-Ni system at mechanical alloying and consequent annealing of elemental powder mixtures, *Physica B* 299 (2001) 236–241.
- [9] Y.V. Baldokhin, V.V. Tcherdyntsev, S.D. Kaloshkin, G.A. Kochetov, Y.A. Pustov, Transformations and fine magnetic structure of mechanically alloyed Fe-Ni alloys, *Journal of Magnetism and Magnetic Materials* 203 (1999) 313–315.
- [10] L.B. Hong, B. Fultz, Two-phase coexistence in Fe-Ni alloys synthesized by ball milling, *Journal of Applied Physics* 79 (1996) 3946–3955.
- [11] J.F. Valderuten, G.A. Perez Alcazar, J.M. Grenèche, Study of Fe-Ni alloys produced by mechanical alloying, *Physica B* 384 (2006) 316–318.
- [12] V.V. Tcherdyntsev, S.D. Kaloshkin, I.A. Tomilin, E.V. Shelekhov, Y.V. Baldokhin, Formation of iron-nickel nanocrystalline alloy by mechanical alloying, *Nanostructured Materials* 12 (1999) 139–142.
- [13] A. Djekoun, A. Otmani, B. Bouzabata, L. Bechiri, N. Randrianantoandro, J.M. Grenèche, Synthesis and characterization of high-energy ball milled nanostructured  $\text{Fe}_{50}\text{Ni}_{50}$ , *Catalysis Today* 113 (2006) 235–239.
- [14] A. Guittoum, A. Layadi, A. Bourzami, H. Tafat, N. Souami, S. Boutarfaia, D. Lacour, X-ray diffraction, microstructure, Mössbauer and magnetization studies of nanostructured  $\text{Fe}_{50}\text{Ni}_{50}$  alloy prepared by mechanical alloying, *Journal of Magnetism and Magnetic Materials* 320 (2008) 1385–1392.
- [15] E. Jartych, J.K. Zurawicz, D. Oleszak, M. Pekala, Magnetic properties and structure of nanocrystalline Fe-Al and Fe-Ni alloys, *Nanostructured Materials* 12 (1999) 927–930.
- [16] R. Hamzaoui, O. Elkedim, N. Fenineche, E. Gaffet, J. Craven, Structure and magnetic properties of nanocrystalline mechanically alloyed Fe-10% Ni and Fe-20% Ni, *Materials Science and Engineering A* 360 (2003) 299–305.
- [17] Y. Liu, J. Zhang, L. Yu, G. Jia, C. Jing, S. Cao, Magnetic and frequency properties for nanocrystalline Fe-Ni alloys prepared by high-energy milling method, *Journal of Magnetism and Magnetic Materials* 285 (2005) 138–144.
- [18] C. Kuhrt, L. Schultz, Phase formation and Martensitic transformation in mechanically alloyed nanocrystalline Fe-Ni, *Journal of Applied Physics* 73 (1993) 1975–1980.
- [19] D. Oleksakova, P. Kollara, J. Fuzera, M. Kusy, S. Roth, K. Polanski, The influence of mechanical milling on structure and soft magnetic properties of NiFe and NiFeMo alloys, *Journal of Magnetism and Magnetic Materials* 316 (2007) 838–841.
- [20] R. Hamzaoui, O. Elkedim, E. Gaffet, Milling conditions effect on structure and magnetic properties of mechanically alloyed Fe-10% Ni and Fe-20% Ni alloys, *Materials Science and Engineering A* 381 (2004) 363–371.
- [21] L.H. Zhu, Q.W. Huang, H.F. Zhao, Effect of nickel content and milling parameters on martensitic transformation of Fe-Ni during mechanical alloying, *Scripta Materialia* 51 (2004) 527–531.
- [22] L.H. Zhu, Q.W. Huang, Study on martensitic transformation of mechanically alloyed nanocrystalline Fe-Ni, *Materials Letters* 57 (2003) 4070–4073.
- [23] R.M. Bozorth, Magnetism, *Reviews of Modern Physics* 19 (1947) 29–86.
- [24] M. Bozorth, The permalloy problem, *Reviews of Modern Physics* 25 (1953) 42–48.
- [25] A.T. English, G.Y. Chin, Metallurgy and magnetic properties control in permalloy, *Journal of Applied Physics* 38 (1967) 1183–1186.
- [26] Y. Zhu, Y. Yang, L. Wei, Z. Zhao, L. Li, Hydrogen storage properties of Mg-Ni-Fe composites prepared by hydriding combustion synthesis and mechanical milling, *Journal of Alloys Compounds* 520 (2012) 207–212.
- [27] P. Palade, S. Sartori, A. Maddalena, G. Principi, S. Lo Russo, M. Lazarescu, G. Schinteie, V. Kuncser, G. Filoti, Hydrogen storage in Mg-Ni-Fe compounds prepared by melt spinning and ball milling, *Journal of Alloys Compounds* 415 (2006) 170–176.
- [28] M.Y. Song, S.H. Baek, J.L. Bobet, S.H. Hong, Hydrogen storage properties of a Mg-Ni-Fe mixture prepared via planetary ball milling in a  $\text{H}_2$  atmosphere, *International Journal of Hydrogen Energy* 35 (2010) 10366–10372.
- [29] S. Helle, M. Pedron, B. Assouli, B. Davis, D. Guay, L. Roué, Structure and high-temperature oxidation behaviour of Cu-Ni-Fe alloys prepared by high-energy ball milling for application as inert anodes in aluminium electrolysis, *Corrosion Science* 52 (2010) 3348–3355.
- [30] B.N. Mondal, A. Basumallick, P.P. Chattopadhyay, Effect of isothermal treatments on the magnetic behavior of nanocrystalline Cu-Ni-Fe alloy prepared by mechanical alloying, *Journal of Magnetism and Magnetic Materials* 309 (2007) 290–294.
- [31] A. Grabias, M. Kopcewicz, D. Oleszak, Phase transformations in the Fe(Co,Ni) ZrB alloys induced by ball milling, *Journal of Alloys and Compounds* 339 (2002) 221–229.
- [32] A. Grabias, D. Oleszak, J. Kalinowska, M. Kopcewicz, J. Latuch, M. Pekala, Structure of the nanocrystalline  $\text{Fe}_{41}\text{Ni}_{20}\text{Co}_{20}\text{Zr}_7\text{B}_{12}$  alloy formed by ball milling, *Journal of Alloys and Compounds* 434–435 (2007) 493–496.

- [33] B.N. Mondal, A. Basumallick, P.P. Chattopadhyay, Magnetic properties of binary  $\text{Cu}_{50}(\text{Ni, Fe and Co})_{50}$  alloys prepared by ball milling and isothermal annealing, *Materials Chemistry and Physics* 110 (2008) 290–294.
- [34] B.N. Mondal, A. Basumallick, D.N. Nath, P.P. Chattopadhyay, Phase evolution and magnetic behaviour of Cu–Ni–Co–Fe quaternary alloys synthesized by ball milling, *Materials Chemistry and Physics* 116 (2009) 358–362.
- [35] W. Maziarz, J. Dutkiewicz, J. Van Humbeeck, T. Czeppe, Processing of nanocrystalline FeAlX (X=Ni, Mn) intermetallics using a mechanical alloying and hot pressing techniques, *Journal of Materials Science* 39 (2004) 5425–5429.
- [36] Z.G. Liu, J.T. Guo, L.Z. Zhou, Z.Q. Hu, M. Umemoto, Mechanical alloying synthesis and structural characterization of ternary Ni–Al–Fe alloys, *Journal of Materials Science* 32 (1997) 4857–4864.
- [37] F. Hadeef, A. Otmani, A. Djekoun, J.M. Grenèche, Structural and microstructural study of nanostructured  $\text{Fe}_{50}\text{Al}_{40}\text{Ni}_{10}$  powders produced by mechanical alloying, *Materials Characterization* 62 (2011) 751–759.
- [38] H.M. Rietveld, Line profiles of neutron powder-diffraction peaks for structure refinement, *Acta Crystallographica* 22 (1967) 151–152.
- [39] F.Z. Bentayeb, S. Alleg, J.M. Grenèche, Structural and microstructural study of Fe–31Cr–12Co mixture prepared by ball milling, *Journal of Alloys and Compounds* 434–435 (2007) 477–480.
- [40] J. Teillet, F. Varret, Université du Maine, Unpublished Mosfit Program.
- [41] M.M. Moshksar, M. Mirzaee, Formation of NiAl intermetallic by gradual and explosive exothermic reaction mechanism during ball milling, *Intermetallics* 12 (2004) 1361–1366.
- [42] B.L. Huang, R.J. Perez, E.J. Lavernia, M.J. Luton, Formation of supersaturated solid solutions by mechanical alloying, *Nanostructured Materials* 7 (1996) 67–79.
- [43] W.B. Pearson, in: P. Villars, L.D. Calvert, (Eds.), *Handbook of Crystallographic Data for Intermetallic Phases*, 1992, ASM, Materials Park, OH, pp. 1038–1039.
- [44] C.T. Stockinger, J.P. Neumann, Determination of order in the intermetallic phase  $\text{Ni}_3\text{Al}$  as a function of temperature, *Journal of Applied Crystallography* 3 (1970) 32–38.
- [45] M.H. Enayati, Z. Sadeghian, M. Salehi, A. Saidi, The effect of milling parameters on the synthesis of  $\text{Ni}_3\text{Al}$  intermetallic compound by mechanical alloying, *Materials Science and Engineering: A* 375–377 (2004) 809–811.
- [46] S.K. Pabi, B.S. Murty, Mechanism of mechanical alloying in Ni–Al and Cu–Zn systems, *Materials Science and Engineering: A* 214 (1996) 146–152.
- [47] F. Cardellini, V. Contini, G. Mazzone, Ordering kinetics of disordered  $\text{Ni}_3\text{Al}$  synthesized by mechanical alloying, *Scripta Metallurgica et Materialia* 2 (1995) 641–646.
- [48] M. Krasnowski, A. Antolak, T. Kulik, Nanocrystalline  $\text{Ni}_3\text{Al}$  alloy produced by mechanical alloying of nickel aluminides and hot-pressing consolidation, *Journal of Alloys and Compounds* 434–435 (2007) 344–347.
- [49] C.Y. Chung, M. Zhu, C.H. Man, Effect of mechanical alloying on the solid state reaction processing of Ni–36.5 at.% Al alloy, *Intermetallics* 10 (2002) 865–871.
- [50] L. Lu, M.O. Lai, S. Zhang, Thermodynamic properties of mechanically alloyed nickel and aluminum powders, *Materials Research Bulletin* 29 (1994) 889–894.
- [51] L. Lu, M.O. Lai, S. Zhang, Thermodynamic properties of mechanically alloyed nickel and aluminum powders, *Journal of Materials Processing Technology* 48 (1995) 683–690.
- [52] N.C. Abhik, R. Vivek, V. Udhayabanu, B.S. Murty, Influence of heat of formation of B2/L1<sub>2</sub> intermetallic compounds on the milling energy for their formation during mechanical alloying, *Journal of Alloys and Compounds* 465 (2008) 106–112.
- [53] A.K. Bhattachaya, E. Arzt, Diffusive reaction during mechanical alloying of intermetallics, *Scripta Metall.* 27 (1992) 635–639.
- [54] C. Suryanarayana, G. Chen, F.H. Froes, Milling maps for phase identification during mechanical alloying, *Scripta Metallurgica* 26 (1992) 1727–1732.
- [55] F. Hadeef, A. Otmani, A. Djekoun, J.M. Grenèche, Nanocrystalline FeAl intermetallics obtained in mechanically alloyed  $\text{Fe}_{50}\text{Al}_{40}\text{Ni}_{10}$  powder, *Superlattices and Microstructures* 49 (2011) 654–665.
- [56] C. Kuhrt, L. Schultz, Formation and magnetic properties of nanocrystalline mechanically alloyed Fe–Co and Fe–Ni, *Journal of Applied Physics* 73 (1993) 6588–6590.
- [57] L. Lutterotti, C.P.D. Maud, Newsletter (IUCr) 24 (2000).
- [58] M. Pekała, D. Oleszak, E. Jartych, J.K. Zurawicz, Structural and magnetic study of mechanically alloyed Fe–Ni, *Nanostructured Materials* 11 (1999) 789–796.
- [59] M. Mhadhbi, M. Khitouni, M. Azabou, A. Kolsi, Characterization of Al and Fe nanosized powders synthesized by high energy mechanical milling, *Materials Characterization* 59 (2008) 944–950.
- [60] K. Zhang, I.V. Alexandrov, K. Lu, The X-ray diffraction study on a nanocrystalline Cu processed by equal-channel angular pressing, *Nanostructured Materials* 9 (1997) 347–350.
- [61] L. Dekhil, S. Alleg, J.J. Sunol, J.M. Grenèche, X-ray diffraction and Mössbauer spectrometry studies of the mechanically alloyed Fe–6P–1.7C powders, *Advanced Powder Metallurgy* 20 (2009) 593–597.
- [62] B. Liu, R. Huang, J. Wang, H.M. Widatallah, H. Lu, Mössbauer investigation of Fe–Ni fine particles, *Journal of Applied Physics* 85 (1999) 1010–1013.
- [63] M. Kadziolka-Gawel, W. Zarek, E. Popiel, A. Chrobak, The crystal structure and magnetic properties of selected fcc FeNi and  $\text{Fe}_{40}\text{Ni}_{40}\text{B}_{20}$  alloys, *Acta Physica Polonica A* 117 (2010) 412–414.
- [64] Y. Zhang, J. Huang, D. Lin, The alloying behavior of boron and carbon in  $\text{Ni}_3\text{Al}$ , *Transactions of Nonferrous Metals Society of China* 7 (1997) 101–105.
- [65] S.W. Du, R.V. Ramanujan, Mechanical alloying of Fe–Ni based nanostructured magnetic materials, *Journal of Magnetism and Magnetic Materials* 292 (2005) 286–298.
- [66] J. Eckert, J.C. Holzer, C.E. Krill III, W.L. Johnson, Mechanically driven alloying and grain size changes in nanocrystalline Fe–Cu powders, *Journal of Applied Physics* 73 (6) (1993) 2794–2802.
- [67] C.E. Johnson, M. Ridoutand, T.E. Cranshaw, The Mössbauer effect in iron alloys, *Proceedings of the Physical Society* 81 (1963) 1079–1090.
- [68] E. Jartych, Local atomic order in nanocrystalline Fe-based alloys obtained by mechanical alloying, *Journal of Magnetism and Magnetic Materials* 265 (2003) 176–188.
- [69] F. Hadeef, A. Otmani, A. Djekoun, J.M. Grenèche, Mössbauer effect study of fine atomic structure of  $\text{Fe}_{50}\text{Al}_{40}\text{Ni}_{10}$  powders, *Superlattices and Microstructures* 51 (2012) 952–958.
- [70] J.M. Grenèche, Magnetic phases in alloys and nanostructured systems, *Hyperfine Interactions* 144/145 (2002) 151–160.
- [71] B. Fultz, H. Kuwano, H. Ouyang, Average widths of grain boundaries in nanophase alloys synthesized by mechanical attrition, *Journal of Applied Physics* 77 (1995) 3458–3466.
- [72] B. Cruz, J.A. Tabares, A. Bohorquez, G.A. Perez Alcazar, A CEMS study of surface oxidation of Fe–Ni alloys, *Hyperfine Interactions* 110 (1997) 7–10.
- [73] Yu.V. Balokhin, P.Ya. Kolotyrykin, Yu.I. Petrov, E.A. Shafranovsky, Some specific features of fine Fe and Fe–Ni particles, *Journal of Applied Physics* 78 (1994) 6496–6498.
- [74] J.Y. Ping, D.G. Rancourt, L.A. Dunlap, Physical basis and break down of hyperfine field distribution analysis in fcc Fe–Ni (5–70 at.%Fe), *Journal of Magnetism and Magnetic Materials* 103 (1992) 285–313.
- [75] H. Okamoto, P.A. Beck, *Magnetische Eigenschaften von Fe<sub>3</sub>Al und FeAl und spezifische Wärmen bei tiefen Temperaturen*, *Monatshefte fuer Chemie* 103 (1972) 907–921.
- [76] H. Ebert, H. Winter, B.L. Gyorffy, D.D. Johnson, F.J. Pinski, Theoretical study of the hyperfine fields of Ni and Fe in FCC Ni(x)Fe(1–x) alloys, *Journal of Physics F* 18 (1988) 719–729.
- [77] M.B. Stearns, Variation of the internal fields and isomer shifts at the Fe sites in the FeAl series, *Journal of Applied Physics* 35 (1964) 1095–1096.
- [78] K. Wolski, G. Le Caer, P. Delcroix, R. Fillit, F. Thévenot, J. Le Cose, Influence of milling conditions on the FeAl intermetallic formation by mechanical alloying, *Materials Science and Engineering: A* 207 (1996) 97–104.
- [79] A. Hanc, G. Dercz, L. Pajak, J.E. Frackowiak, J. Kansy, Mössbauer and structure studies on metallic powders from Fe–Al–X (X=Ni, Cu, Cr), *Archives of Materials Science and Engineering* 31 (2008) 21–24.
- [80] E. Lima Jr., V. Drago, R. Bolsoni, P.F.P. Fichtner, nanostructured  $\text{Fe}_{50}\text{Ni}_{50}$  alloy formed by chemical reduction, *Solid State Communications* 125 (2003) 265–270.